

EXACT STIFFNESS METHOD FOR QUASI-STATICS OF A MULTI-LAYERED POROELASTIC MEDIUM

T. SENJUNTICHAJ and R. K. N. D. RAJAPAKSE

Department of Civil and Geological Engineering, University of Manitoba, Winnipeg,
Canada R3T 2N2

(Received 13 December 1993; in revised form 28 July 1994)

Abstract—A method is presented to study the three-dimensional quasi-static response of a multi-layered poroelastic half-space with compressible constituents. The system under consideration consists of N layers of different thickness and material properties overlying a homogeneous half-space. Fourier expansion, Laplace transforms and Hankel transforms with respect to the circumferential, time and radial coordinates, respectively, are used in the formulation. Laplace–Hankel transforms of displacements and pore pressure at layer interfaces are considered as the basic unknowns. Exact stiffness matrices describing the relationship between generalized displacement and force vectors of a finite layer and a half-space are derived explicitly in the transform space. The global stiffness matrix of a layered system is assembled by considering the continuity of tractions and fluid flow at layer interfaces. The time histories of displacements, stresses and pore pressure are obtained by solving the stiffness equation system for discrete values of Laplace and Hankel transform parameters, and using numerical quadrature schemes for Laplace and Hankel transform inversions. Selected numerical results for different layered systems are presented to portray the influence of layering and poroelastic material properties. The advantage of the present method is that for an N -layered system, it yields a numerically stable symmetric stiffness matrix of order $4N \times 4N$ when compared to the unsymmetric and numerically unstable coefficient matrix of order $8N \times 8N$ associated with the conventional method based on the determination of layer arbitrary coefficients.

INTRODUCTION

The theory of poroelasticity has its origin in the one-dimensional theory of soil consolidation proposed by Terzaghi (1923). Biot (1941) developed a general theory of three-dimensional consolidation of fluid-saturated porous elastic solids by adopting Terzaghi's concepts. Later, Rice and Cleary (1976) reformulated Biot's work in terms of material constants which are more easily identifiable. Over the last forty years, Biot's theory has been the basis for analysis of a variety of geotechnical and geophysical problems related to poroelastic regions, e.g. soil consolidation (McNamee and Gibson, 1960; Schiffman and Fungaroli, 1965; Rajapakse and Senjuntichai, 1993), borehole problems (Detournay and Cheng, 1988; Rajapakse, 1993), hydraulic fracture (Rice and Cleary, 1976; Detournay *et al.*, 1989) and earth faulting (Rice and Cleary, 1976; Rudnicki, 1986, 1987).

An important class of problems encountered in geomechanics, energy resource explorations, biomechanics, etc. is concerned with the study of the mechanical response of multilayered media since it represents a closer approximation to most physical systems such as natural soil profiles, which are normally layered in character. Analytical solutions to two- and three-layered ideal elastic media have been presented in the past by applying integral transform techniques (Burmister, 1945; Chan *et al.*, 1974). The use of numerical quadrature in the evaluation of elastic fields is unavoidable unless approximations are made in the evaluation of semi-infinite integrals associated with the inverse integral transforms. A finite element approach combined with the far-field behaviour of elastic fields has been proposed to study the response of a layered ideal elastic half-space (Muki and Dong, 1980; Rajapakse and Karasudhi, 1985). An approach which is quite similar to the classical finite element method has been presented by Waas (1972) to analyze layered ideal elastic media. In this approach, a multi-layered half-space is divided into a number of thin layers within which the displacements have prescribed variations in the vertical direction (e.g. linear). An approximate stiffness matrix is derived for each layer on the basis of the assumed

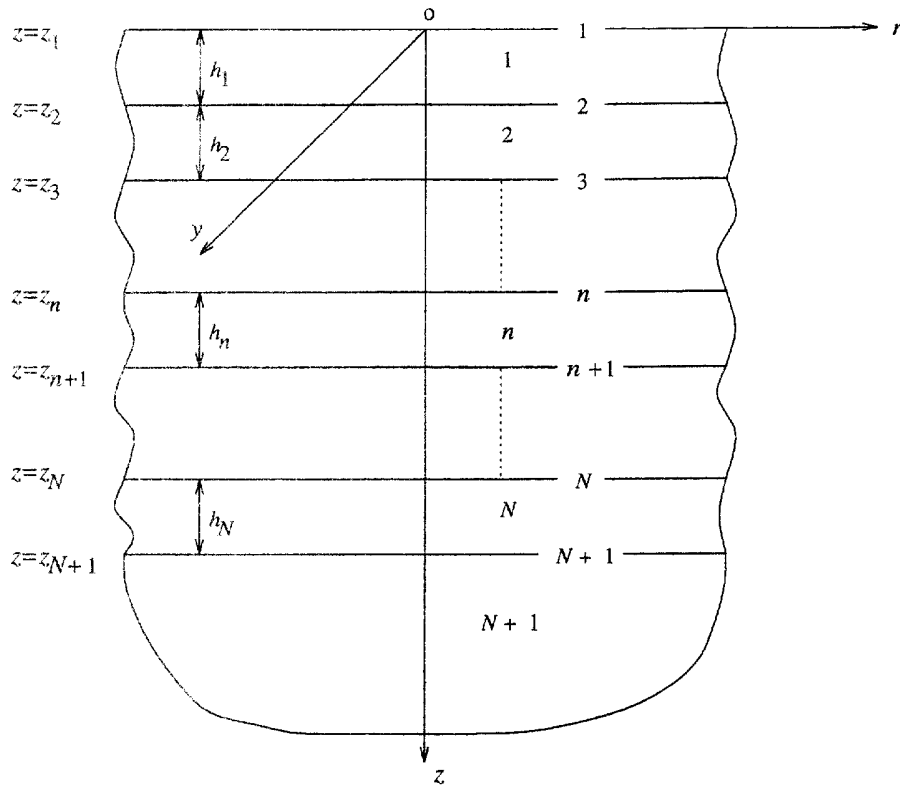


Fig. 1. Geometry of a multi-layered half-space.

displacement representation and a global stiffness matrix of the system is obtained by assembling layer stiffness matrices. Further approximations are required in this scheme to include an underlying half-space. The approximate scheme of Waas (1972) has been used in the past to study static and dynamic responses of layered ideal elastic materials (Kausel and Peek, 1982; Kausel and Scale, 1987).

The conventional method to evaluate the response of a system with N layers, while rigorously satisfying the governing equations, is based on the determination of arbitrary functions corresponding to each layer numerically (Thomson, 1950; Haskell, 1953). In this approach, analytical general solutions of each layer expressed in terms of a set of arbitrary functions in Fourier or Hankel transform space are used to establish a linear simultaneous equation system with arbitrary functions as the unknowns by considering the boundary conditions at top surface and continuity conditions at layer interfaces. The equation system is solved numerically for discrete values of the integral transform parameter and the response is computed by applying numerical quadrature to evaluate the inverse transform integrals. Vardoulakis and Harnpattanapanich (1986) used the above approach to evaluate the quasi-static response of a layered poroelastic medium with incompressible constituents. The incompressibility of constituents is an approximation which is valid mainly for soils but not for porous rocks. The conventional scheme based on the determination of layer arbitrary coefficients results in an unsymmetric matrix of order $(8N+4) \times (8N+4)$ for a layered poroelastic system as shown in Fig. 1 which needs to be repetitively solved in the numerical evaluation of the response. The numerical effort involved in the analysis is substantially high due to the presence of the Laplace inversion in addition to the Fourier or Hankel transform inversion (Vardoulakis and Harnpattanapanich, 1986). In addition, the elements of the coefficient matrix involve both negative and positive exponentials of the Fourier/Hankel transform parameter which results in numerically ill-conditioned matrices for increasing values of the transform parameter. These ill-conditioned matrices yield spurious contributions in the numerical evaluation of the response.

In recent years, exact stiffness matrix methods have been presented to study the response of multi-layered media. Booker and Small (1987) considered layered soil consolidation problems by using a stiffness matrix method based on analytical solutions for a medium with incompressible constituents. Choi and Thangjitham (1991), Rajapakse and Wang (1992) and Wang and Rajapakse (1994) considered static and dynamic stress analysis of layered anisotropic elastic media by using exact stiffness matrix schemes. This paper is a further development of three-dimensional solutions presented by Rajapakse and Senjuntichai (1993) for a homogeneous poroelastic medium with compressible constituents. The main objective is to develop a computationally efficient and numerically stable exact stiffness matrix scheme to evaluate the quasi-static response of a multi-layered poroelastic medium with *compressible* constituents. In the present approach, the Laplace-Hankel transforms of displacements and pore pressure at layer interfaces are considered as the basic unknowns. The three-dimensional general solutions given by Rajapakse and Senjuntichai (1993) are used to construct explicitly an 8×8 symmetric stiffness matrix which describes the relationship between generalized displacement and force vectors of a layer. For an underlying half-space, a 4×4 exact stiffness matrix is also derived by using the general solutions. The global stiffness matrix of a multi-layered half-space is assembled by considering the continuity conditions of tractions and fluid flow at the interface between the adjacent layers. The numerical solution of the global stiffness equation for discrete values of Hankel and Laplace transform parameters results in the Laplace-Hankel transforms of displacements and pore pressure at layer interfaces. Thereafter, time domain solutions for displacements, stresses, pore pressure and fluid discharge are computed by applying a numerical scheme for Laplace inversion and direct numerical quadrature for Hankel transform inversion. The present method has high numerical efficiency due to the fact that it involves the solution of a banded symmetric stiffness matrix of nearly one-half the size of the unsymmetric coefficient matrix corresponding to the conventional scheme based on the determination of layer arbitrary coefficients. In addition, the elements of the stiffness matrix involve only numerically stable negative exponential terms of Hankel transform parameters resulting in well-conditioned matrices.

BASIC EQUATIONS AND GENERAL SOLUTIONS

The constitutive relations of a homogeneous poroelastic material with compressible constituents can be expressed with respect to a conventional cylindrical polar coordinate system (r, θ, z) by using the standard indicial notation as (Rice and Cleary, 1976)

$$\sigma_{ij} = 2\mu \left[\varepsilon_{ij} + \frac{\nu}{1-2\nu} \delta_{ij} \varepsilon \right] - \frac{3(\nu_u - \nu)}{B(1-2\nu)(1+\nu_u)} \delta_{ij} p, \quad i, j = r, \theta, z. \quad (1)$$

In the above equation, σ_{ij} is the total stress component of the bulk material; ε_{ij} and ε are the strain component and the dilatation of the solid matrix, respectively; p is the excess pore fluid pressure (suction is considered negative); μ , ν and ν_u are the shear modulus, drained and undrained Poisson's ratios, respectively; B is the Skempton's pore pressure coefficient (Skempton, 1954) and δ_{ij} is the Kronecker delta. It is noted that $0 \leq B \leq 1$ and $\nu \leq \nu_u \leq 0.5$ for all poroelastic materials. The limiting cases of a poroelastic solid with incompressible constituents and a dry elastic material are obtained when $\nu_u = 0.5$ and $B = 1$, and $B \rightarrow 0$, respectively. The excess pore fluid pressure can be expressed as

$$p = -\frac{2\mu B(1+\nu_u)}{3(1-2\nu_u)} \varepsilon + \frac{2\mu B^2(1-2\nu)(1+\nu_u)^2}{9(1-2\nu_u)(\nu_u - \nu)} \zeta \quad (2)$$

where ζ is the variation of fluid volume per unit reference volume. Let u_i and w_i denote the average displacement of the solid matrix and the fluid displacement relative to the solid matrix, respectively, in the i -direction ($i = r, \theta, z$). Then,

$$w_i = \int_0^r q_i dt \quad (3)$$

where q_i is the fluid discharge in the i -direction defined as

$$q_i = -\kappa \frac{\partial p}{\partial i}, \quad i = r, z \quad \text{and} \quad q_\theta = -\kappa \frac{\partial p}{r \partial \theta}. \quad (4)$$

In addition, κ is the coefficient of permeability defined as the ratio between the intrinsic permeability of the medium and the viscosity of the constituents.

Application of the Fourier expansion with respect to the circumferential coordinate θ for displacements u_i and pore pressure p results in

$$u_i(r, \theta, z, t) = \sum_{m=0}^{\infty} u_{im}(r, z, t) f(\theta) - \sum_{m=0}^{\infty} \check{u}_{im}(r, z, t) f'(\theta) \quad (5)$$

$$p(r, \theta, z, t) = \sum_{m=0}^{\infty} p_m(r, z, t) \cos m\theta + \sum_{m=0}^{\infty} \check{p}_m(r, z, t) \sin m\theta \quad (6)$$

where

$$f(\theta) = \begin{cases} \cos m\theta, & i \neq \theta, \\ \sin m\theta, & i = \theta. \end{cases} \quad (7)$$

In eqns (5) and (6), u_{im} and p_m are symmetric components and \check{u}_{im} and \check{p}_m are anti-symmetric components corresponding to the m th harmonic. $f'(\theta)$ denotes the derivative of $f(\theta)$ with respect to the circumferential coordinate θ . In the subsequent analysis, only symmetric components are considered without loss of generality.

The Laplace–Hankel transform (m th order) of function $\phi(r, z, t)$ with respect to the variables t and r , respectively, is defined by (Sneddon, 1951)

$$\mathcal{H}_m\{\phi(r, z, t)\} = \int_0^\infty \int_0^\infty \phi(r, z, t) e^{-st} J_m(\xi r) r dr dt. \quad (8)$$

In eqn (8), s and ξ denote the Laplace and Hankel transform parameters respectively, and J_m denotes the Bessel function of the first kind of order m . The inverse relationship is given by

$$\phi(r, z, t) = \frac{1}{2\pi i} \int_{\alpha-i\infty}^{\alpha+i\infty} \int_0^\infty \mathcal{H}_m[\phi(r, z, t)] e^{st} J_m(\xi r) \xi d\xi ds \quad (9)$$

where α is greater than the real part of all singularities of $\mathcal{H}_m[\phi(r, z, t)]$ and $i = \sqrt{-1}$.

It can be shown that general solutions for the m th harmonic of solid and fluid displacements, pore pressure and stresses in the Laplace–Hankel transform space (Rajapakse and Senjuntichai, 1993) can be expressed in the following matrix form

$$\mathbf{v}(\xi, z, s) = \mathbf{R}(\xi, z, s) \mathbf{C}(\xi, s) \quad (10)$$

$$\mathbf{f}(\xi, z, s) = \mathbf{S}(\xi, z, s) \mathbf{C}(\xi, s) \quad (11)$$

where

$$\mathbf{v}(\xi, z, s) = \langle v_i(\xi, z, s) \rangle^T, \quad i = 1, 2, 3, 4 \quad (12)$$

$$\mathbf{f}(\xi, z, s) = \langle f_i(\xi, z, s) \rangle^T, \quad i = 1, 2, 3, 4 \quad (13)$$

$$v_1(\xi, z, s) = \frac{1}{2} [\bar{\mathcal{H}}_{m+1}(u_{rm} + u_{0m}) - \bar{\mathcal{H}}_{m-1}(u_{rm} - u_{0m})] \quad (14)$$

$$v_2(\xi, z, s) = \frac{1}{2} [\bar{\mathcal{H}}_{m+1}(u_{rm} + u_{0m}) + \bar{\mathcal{H}}_{m-1}(u_{rm} - u_{0m})] \quad (15)$$

$$v_3(\xi, z, s) = \bar{\mathcal{H}}_m(u_{zm}) \quad (16)$$

$$v_4(\xi, z, s) = \bar{\mathcal{H}}_m(p_m) \quad (17)$$

$$f_1(\xi, z, s) = \frac{1}{2} [\bar{\mathcal{H}}_{m+1}(\sigma_{zrm} + \sigma_{z0m}) - \bar{\mathcal{H}}_{m-1}(\sigma_{zrm} - \sigma_{z0m})] \quad (18)$$

$$f_2(\xi, z, s) = \frac{1}{2} [\bar{\mathcal{H}}_{m+1}(\sigma_{zrm} + \sigma_{z0m}) + \bar{\mathcal{H}}_{m-1}(\sigma_{zrm} - \sigma_{z0m})] \quad (19)$$

$$f_3(\xi, z, s) = \bar{\mathcal{H}}_m(\sigma_{zzm}) \quad (20)$$

$$f_4(\xi, z, s) = \bar{\mathcal{H}}_m(w_{zm}) \quad (21)$$

$$\mathbf{C} = \langle A_m \ B_m \ C_m \ D_m \ E_m \ F_m \ G_m \ H_m \rangle^T \quad (22)$$

and the matrices $\mathbf{R}(\xi, z, s)$ and $\mathbf{S}(\xi, z, s)$ are defined in the Appendix. The arbitrary functions $A_m(\xi, s)$, $B_m(\xi, s)$, \dots , $H_m(\xi, s)$ appearing in $\mathbf{C}(\xi, s)$ are to be determined by employing appropriate boundary and/or continuity conditions. In the ensuing sections, a computationally efficient exact stiffness matrix scheme is presented to study the quasi-static response of a multi-layered poroelastic half-space as an effective alternative to the conventional method based on the determination of the layer arbitrary coefficient vector $\mathbf{C}(\xi, s)$.

STIFFNESS MATRICES

A multi-layered system with a total of N poroelastic layers overlying a poroelastic half-space is considered in this section. Layers and interfaces are numbered as shown in Fig. 1. A superscript “ n ” is used to denote quantities associated with the n th layer ($n = 1, 2, \dots, N$). For an n th layer, the following relationships can be established by using eqns (10) and (11)

$$\mathbf{U}^{(n)} = \begin{bmatrix} \mathbf{R}^{(n)}(\xi, z_n, s) \\ \dots\dots\dots \\ \mathbf{R}^{(n)}(\xi, z_{n+1}, s) \end{bmatrix} \mathbf{C}^{(n)} \quad (23)$$

$$\mathbf{F}^{(n)} = \begin{bmatrix} -\mathbf{S}^{(n)}(\xi, z_n, s) \\ \dots\dots\dots \\ \mathbf{S}^{(n)}(\xi, z_{n+1}, s) \end{bmatrix} \mathbf{C}^{(n)} \quad (24)$$

where

$$\mathbf{U}^{(n)} = \langle \mathbf{v}^{(n)}(\xi, z_n, s) \quad \mathbf{v}^{(n)}(\xi, z_{n+1}, s) \rangle^T \quad (25)$$

$$\mathbf{F}^{(n)} = \langle -\mathbf{f}^{(n)}(\xi, z_n, s) \quad \mathbf{f}^{(n)}(\xi, z_{n+1}, s) \rangle^T. \quad (26)$$

In eqns (23)–(26), $\mathbf{U}^{(n)}$ denotes a vector of generalized coordinates for the n th layer whose elements are related to the Laplace–Hankel transforms of the m th Fourier harmonic of

displacements and pore pressure of the top and bottom surfaces of the n th layer. Similarly, $\mathbf{F}^{(n)}$ denotes a generalized force vector whose elements are related to the Laplace–Hankel transforms of the m th Fourier harmonic of tractions and fluid displacements of the top and bottom surfaces of the n th layer. The matrices $\mathbf{R}^{(n)}$ and $\mathbf{S}^{(n)}$ in eqns (23) and (24) are identical to \mathbf{R} and \mathbf{S} defined in the Appendix except that the material properties of the n th layer are used in the definition and $z = z_n$ and z_{n+1} . The vector $\mathbf{C}^{(n)}$ is the arbitrary coefficients vector corresponding to the n th layer.

Equation (23) can be inverted to express $\mathbf{C}^{(n)}$ in terms of $\mathbf{U}^{(n)}$ and the substitution in eqn (24) yields

$$\mathbf{F}^{(n)} = \mathbf{K}^{(n)}\mathbf{U}^{(n)}, \quad n = 1, 2, \dots, N \tag{27}$$

where $\mathbf{K}^{(n)}$ can be considered as an exact stiffness matrix in the Laplace–Hankel transform space describing the relationship between the generalized displacement vector $\mathbf{U}^{(n)}$ and the force vector $\mathbf{F}^{(n)}$ for the n th layer.

The explicit derivation of $\mathbf{K}^{(n)}$ corresponding to an arbitrary Fourier harmonic of a three-dimensional poroelastic problem is extremely complicated and it is impossible to achieve this task manually due to the fact that the inversion of eqn (23) involves a fully populated 8×8 unsymmetric matrix whose elements involve rather complicated expressions. However, this task, which needs to be performed only once, can be achieved by using modern symbolic manipulation packages. In the present study, authors used the computer algebra package *Mathematica* (Wolfram, 1988) to obtain $\mathbf{K}^{(n)}$ explicitly. *Mathematica* results in extremely lengthy and complicated expressions for elements of $\mathbf{K}^{(n)}$ which have to be extensively manipulated and reduced to obtain more simplified expressions to achieve a computationally efficient solution scheme. After lengthy manipulations, it is found that $\mathbf{K}^{(n)}$ is symmetric and its elements can be expressed as

1st Row:

$$k_{11} = (\alpha_{2n}^2 + 1)(d_1\chi_1 - d_2\chi_2) - 4\alpha_{2n}(d_3\chi_1 - d_4\chi_3) \tag{28}$$

$$k_{12} = 0, \quad k_{13} = (\alpha_{2n}^2 - 1)(d_1\chi_1 - d_2\chi_2) + \xi \tag{29}$$

$$k_{14} = \delta_1(\alpha_{2n}^2 - 1)(d_6\chi_2 - d_5\chi_1 - 4\alpha_{1n}\alpha_{2n}\chi_3) + \delta_2k_{11} \tag{30}$$

$$k_{15} = 2d_7\chi_1 - 2\alpha_{2n}(2d_1\chi_1 - d_2\chi_2 + d_5\chi_3) \tag{31}$$

$$k_{16} = 0, \quad k_{17} = 2(\alpha_{2n}^2 - 1)[d_4\chi_3 - d_3\chi_1] \tag{32}$$

$$k_{18} = 2\delta_1[\alpha_{2n}(d_2\chi_1 + d_6\chi_3) - d_7\chi_2] + \delta_2k_{15} \tag{33}$$

where

$$\alpha_{1n} = e^{-\gamma h_n}, \quad \alpha_{2n} = e^{-\xi h_n}, \quad \gamma = \left(\xi^2 + \frac{s}{c}\right)^{1/2} \tag{34}$$

$$d_1 = (\alpha_{1n}\alpha_{2n} - 1)^2 + (\alpha_{1n} - \alpha_{2n})^2, \quad d_2 = (\alpha_{1n}\alpha_{2n} - 1)^2 - (\alpha_{1n} - \alpha_{2n})^2 \tag{35}$$

$$d_3 = (\alpha_{1n}\alpha_{2n} - 1)(\alpha_{2n} - \alpha_{1n}), \quad d_4 = \alpha_{2n}(\alpha_{1n}^2 - 1) \tag{36}$$

$$d_5 = (\alpha_{1n}^2 - 1)(\alpha_{2n}^2 + 1), \quad d_6 = (\alpha_{1n}^2 + 1)(\alpha_{2n}^2 - 1), \quad d_7 = \alpha_{1n}(\alpha_{2n}^2 - 1)^2 \tag{37}$$

$$\chi_1 = \frac{4\mu^2}{R}(a_3^2 a_4^2 \eta \delta_1), \quad \chi_2 = \frac{2\mu}{\xi R}(2\mu a_3^2 a_4^2 \xi \eta \delta_2 - a_2 a_3^2 a_4), \quad \chi_3 = \frac{2\mu}{R}(a_1 a_3^2 a_4 h_n) \tag{38}$$

$$R = (\alpha_{2n}^2 - 1)(2d_1 g_1 - d_2 g_2) - 4\alpha_{2n}(2d_3 g_3 - d_4 g_4) \tag{39}$$

$$g_1 = \frac{2\mu a_3 \eta}{\xi} [2\mu a_3 a_4^2 \xi \eta \delta_1 \delta_2 - a_2 a_3 a_4 \delta_1] \tag{40}$$

$$g_2 = \frac{1}{\xi^2} [a_2^2 a_3^2 - 4\mu a_3^2 a_4 \eta \{a_2 \delta_2 - \mu a_4 \eta (\delta_1^2 + \delta_2^2)\}] \quad (41)$$

$$g_3 = 2\mu a_1 a_3^2 a_4 \eta \delta_1 h_n, \quad g_4 = a_1^2 a_3^2 h_n^2 \quad (42)$$

and $a_i (i = 1, 4)$, c , η and $\delta_i (i = 1, 2)$ are defined in eqns (86) and (87) in the Appendix.

2nd Row :

$$k_{22} = -\mu \xi \frac{(\alpha_{2n}^2 + 1)}{(\alpha_{2n}^2 - 1)}, \quad k_{26} = \frac{2\mu \xi \alpha_{2n}}{(\alpha_{2n}^2 - 1)} \quad (43)$$

$$k_{2i} = 0, \quad i = 1, 3, 4, 5, 7, 8. \quad (44)$$

3rd Row :

$$k_{33} = (\alpha_{2n}^2 - 1)(d_6 \chi_1 - d_5 \chi_2) - 4\alpha_{2n} d_4 \chi_3 \quad (45)$$

$$k_{34} = (\alpha_{2n}^2 - 1) \{ \delta_1 (d_1 \chi_2 - d_2 \chi_1) + \delta_2 (d_1 \chi_1 - d_2 \chi_2) \} - 4\alpha_{2n} \delta_1 d_3 \chi_3 \quad (46)$$

$$k_{35} = -k_{17}, \quad k_{36} = 0, \quad k_{37} = 2\alpha_{2n} (d_2 \chi_2 + d_5 \chi_3) - 2d_7 \chi_1 \quad (47)$$

$$k_{38} = 2\delta_1 [\alpha_{2n} d_1 \chi_3 - (\alpha_{2n}^2 - 1) d_3 \chi_2] + \delta_2 k_{35}. \quad (48)$$

4th Row :

$$k_{44} = (\alpha_{2n}^2 + 1)(2d_1 \psi_2 - d_2 \psi_1) - (\alpha_{2n}^2 - 1)d_6 \psi_3 + 4\alpha_{2n} \psi_4 \quad (49)$$

$$k_{45} = k_{18}, \quad k_{46} = 0, \quad k_{47} = -k_{38} \quad (50)$$

$$k_{48} = 2d_7 \psi_3 - 2\alpha_{2n} (2d_1 \psi_2 - d_2 \psi_1 + \psi_5) \quad (51)$$

where

$$\psi_1 = \frac{2\mu a_3}{\xi R} [a_2 a_3 a_4 (\delta_1^2 - \delta_2^2) + 2\mu a_3 a_4^2 \xi \eta \delta_2 (\delta_1^2 + \delta_2^2)] \quad (52)$$

$$\psi_2 = \frac{4\mu^2}{R} (a_3^2 a_4 \eta \delta_1 \delta_2^2), \quad \psi_3 = \frac{a_2^2 a_3^2 \delta_1}{\xi^2 \eta R} \quad (53)$$

$$\psi_4 = \frac{1}{\eta \delta_1 R} [d_4 g_3 (\delta_1^2 + \delta_2^2) - 2\alpha_{1n} (\alpha_{2n}^2 - 1) \delta_1 \delta_2 g_3 + \alpha_{2n} (\alpha_{1n}^2 + 1) \delta_1^2 g_4] \quad (54)$$

$$\psi_5 = \frac{1}{\eta \delta_1 R} [d_5 g_3 (\delta_1^2 + \delta_2^2) - 2d_6 \delta_1 \delta_2 g_3 + 4\alpha_{1n} \alpha_{2n} \delta_1^2 g_4]. \quad (55)$$

5th Row :

$$k_{55} = k_{11}, \quad k_{56} = 0, \quad k_{57} = -k_{13}, \quad k_{58} = k_{14}. \quad (56)$$

6th Row :

$$k_{66} = k_{22}, \quad k_{67} = k_{68} = 0. \quad (57)$$

7th Row :

$$k_{77} = k_{33}, \quad k_{78} = -k_{34}. \quad (58)$$

8th Row :

$$k_{88} = k_{44}. \quad (59)$$

It is noted that the layer stiffness matrix $\mathbf{K}^{(n)}$ is a function of the layer thickness, the layer material properties, the Laplace and Hankel transform parameters s and ξ . Only negative exponentials that decrease rapidly with increasing ξ , s and h_n are involved in k_{ij} . It should be noted that relationships between k_{ij} s [e.g. eqns (56)–(59)] can also be derived on the basis of the physical behaviour of the system since each k_{ij} represents a component of a generalized force vector due to a generalized displacement vector equal to a unit vector. When compared to the stiffness matrix method proposed by Waas (1972), the $\mathbf{K}^{(n)}$ obtained from the present method is exact and do not involve any approximations in the derivation.

For the underlying half-space, due to the regularity condition at $z \rightarrow \infty$, the general solutions involve only four arbitrary coefficients in the vector $\mathbf{C}^{(n)}$, i.e. $B_m^{(N+1)}$, $D_m^{(N+1)}$, $F_m^{(N+1)}$ and $H_m^{(N+1)}$. The stiffness matrix of the bottom half-space can be expressed as

$$\mathbf{F}^{(N+1)} = \mathbf{K}^{(N+1)} \mathbf{U}^{(N+1)} \quad (60)$$

where

$$\mathbf{U}^{(N+1)} = \langle \mathbf{v}^{(N+1)}(\xi, z_{N+1}, s) \rangle^T \quad (61)$$

$$\mathbf{F}^{(N+1)} = \langle -\mathbf{f}^{(N+1)}(\xi, z_{N+1}, s) \rangle^T \quad (62)$$

and

$$\mathbf{K}^{(N+1)} = \text{symm.}[\tilde{k}_{ij}]_{4 \times 4}. \quad (63)$$

The elements in the half-space stiffness matrix can be expressed as

$$\tilde{k}_{11} = -\frac{2\mu a_3 a_4 \eta}{\beta}, \quad \tilde{k}_{12} = 0 \quad (64)$$

$$\tilde{k}_{13} = -\frac{\mu a_3 \eta}{\beta} + 2\xi(\delta_1 - \delta_2)\tilde{k}_{11}, \quad \tilde{k}_{14} = (\delta_2 - \delta_1)\tilde{k}_{11} \quad (65)$$

$$\tilde{k}_{22} = \mu\xi, \quad \tilde{k}_{23} = \tilde{k}_{24} = 0 \quad (66)$$

$$\tilde{k}_{33} = \tilde{k}_{11}, \quad \tilde{k}_{34} = -\tilde{k}_{14} \quad (67)$$

$$\tilde{k}_{44} = \frac{a_2 a_3 c \delta_1}{\xi \beta} + c \delta_2 \tilde{k}_{14} \quad (68)$$

where

$$\beta = 2\mu a_3 a_4 \eta^2 (\delta_2 - \delta_1) - \frac{a_2 a_3 \eta}{\xi}. \quad (69)$$

It is noted that exponential terms of ξ and s are not involved in the expression of $\mathbf{K}^{(N+1)}$ and its elements depend on the material properties of the underlying half-space, the Laplace and Hankel transform parameters s and ξ , respectively. The stiffness matrix $\mathbf{K}^{(N+1)}$ of the underlying half-space exactly satisfies all the governing equations.

GLOBAL STIFFNESS MATRIX

The global stiffness matrix of a multi-layered half-space is assembled by using the layer and half-space stiffness matrices together with the continuity conditions of tractions and fluid flow at layer interfaces. For example, the continuity conditions at the n th interface can be expressed as

$$\mathbf{f}^{(n-1)}(\xi, z_n, s) - \mathbf{f}^{(n)}(\xi, z_n, s) = \mathbf{T}^{(n)} \tag{70}$$

where $\mathbf{f}^{(n)}$ is identical to \mathbf{f} defined in eqn (13) with superscript “ n ” denoting the layer number and

$$\mathbf{T}^{(n)} = \left\langle T_1^{(n)} \quad T_2^{(n)} \quad T_3^{(n)} \quad \frac{Q^{(n)}}{s} \right\rangle^T \tag{71}$$

in which

$$T_1^{(n)} = \frac{1}{2} [\bar{\mathcal{H}}_{m+1}(T_{rm}^{(n)} + T_{\theta m}^{(n)}) - \bar{\mathcal{H}}_{m-1}(T_{rm}^{(n)} - T_{\theta m}^{(n)})] \tag{72}$$

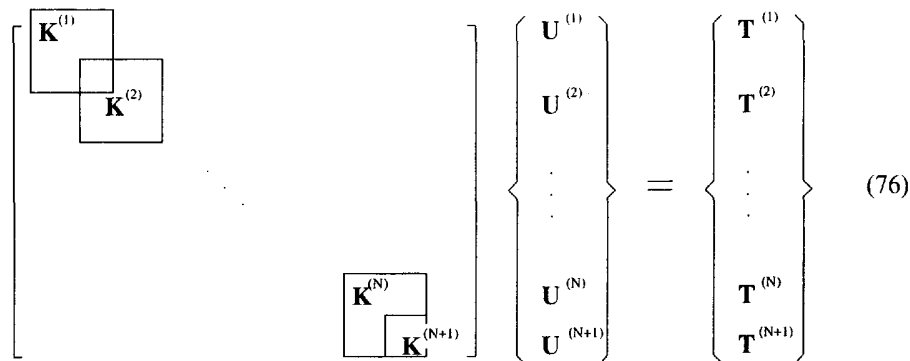
$$T_2^{(n)} = \frac{1}{2} [\bar{\mathcal{H}}_{m+1}(T_{rm}^{(n)} + T_{\theta m}^{(n)}) + \bar{\mathcal{H}}_{m-1}(T_{rm}^{(n)} - T_{\theta m}^{(n)})] \tag{73}$$

$$T_3^{(n)} = \bar{\mathcal{H}}_m(T_{zm}^{(n)}) \tag{74}$$

$$Q^{(n)} = \bar{\mathcal{H}}_m(Q_m^{(n)}) \tag{75}$$

where $T_m^{(n)} (i = r, \theta, z)$ and $Q_m^{(n)}$ denote the m th Fourier harmonic of the tractions and fluid source applied at the n th interface, respectively.

The consideration of eqn (70) at each layer interface together with eqns (27) and (60) results in the following global equation system



$$\left[\begin{array}{c} \mathbf{K}^{(1)} \\ \mathbf{K}^{(2)} \\ \vdots \\ \mathbf{K}^{(N)} \\ \mathbf{K}^{(N+1)} \end{array} \right] \begin{Bmatrix} \mathbf{U}^{(1)} \\ \mathbf{U}^{(2)} \\ \vdots \\ \mathbf{U}^{(N)} \\ \mathbf{U}^{(N+1)} \end{Bmatrix} = \begin{Bmatrix} \mathbf{T}^{(1)} \\ \mathbf{T}^{(2)} \\ \vdots \\ \mathbf{T}^{(N)} \\ \mathbf{T}^{(N+1)} \end{Bmatrix} \tag{76}$$

The global stiffness matrix of eqn (76) is a well-conditioned symmetric matrix and has a band width equal to 8. It is naturally constrained against rigid body displacements due to the presence of $\mathbf{K}^{(N+1)}$. If a half-space is not present at the bottom then the bottom plane at $z = z_N$ has to be restrained to eliminate the rigid body displacements. The number of unknowns in the final equation system, i.e. eqn (76) is equal to $4(N+1)$ which is nearly one-half of that corresponding to the classical approach based on the solution of layer arbitrary coefficients $A_m^{(n)}, B_m^{(n)}, \dots, H_m^{(n)}$. This reduction of the size of the final equation system together with the symmetry makes the present scheme computationally more efficient than the conventional scheme (Vardoulakis and Harnpattanapanich, 1986). Furthermore, eqn (76) is invertible and numerically stable for very large values of ξ .

The Laplace–Hankel transforms of stresses and fluid discharge at the top and bottom interfaces of a layer can be obtained by using eqns (9), (27) and (76). If displacements and/or pore pressure within points of a layer are required then it is convenient to define a set of fictitious planes through these points and consider these as additional layers. Alternatively, eqn (23) can be used to compute $\mathbf{C}^{(n)}$ for a layer and thereafter compute displacements and pore pressure at an arbitrary point within a layer using eqn (10). This, however, may involve the inversion of numerically ill-conditioned matrices such as $\mathbf{R}^{(n)}$ for large values of ξ and consequently loss of precision. If loads and/or fluid sources are applied within a layer then fictitious interfaces are considered at the loading levels.

NUMERICAL RESULTS AND DISCUSSION

Numerical scheme

Since eqn (76) yields the Laplace–Hankel transforms of displacements and pore pressure at layer interfaces for discrete values of ξ and s , the response of the half-space is determined by numerically evaluating the integrals appearing in eqn (9). The Laplace inversion is carried out numerically and the integral with respect to ξ in eqn (9) is evaluated by using numerical quadrature. A review of the literature indicates that the Laplace inversion can be carried out very accurately (Piessens, 1975) by using the numerical Laplace inversion method proposed by Stehfest (1970). The formula due to Stehfest is given by

$$f(t) \approx \frac{\ln 2}{t} \sum_{n=1}^N c_n \bar{f}\left(n \frac{\ln 2}{t}\right) \quad (77)$$

where \bar{f} denotes the Laplace transform of $f(t)$ and

$$c_n = (-1)^{n+N/2} \sum_{k=\lfloor (n+1)/2 \rfloor}^{\min(n, N/2)} \frac{k^{N/2} (2k)!}{(N/2 - k)! k! (k-1)! (n-k)! (2k-n)!} \quad (78)$$

and N is even. It is found that accurate time-domain solutions are obtained from eqn (77) with $N \geq 6$ for poroelasticity problems (Detournay and Cheng, 1988 and Rajapakse and Senjuntichai, 1993). It is important to note that the Stehfest method is computationally quite demanding although it is accurate. A more simple and computationally efficient scheme is given by Schapery (1962) which can be expressed as

$$f(t) \approx [s \bar{f}]_{s=0.5/t} \quad (79)$$

where \bar{f} denotes the Laplace transform of $f(t)$ and s is the Laplace transform parameter.

A computer code based on the solution procedure described in the preceding sections has been developed to investigate the quasi-static behaviour of a multi-layered poroelastic half-space. The tasks performed by the computer code can be described as (1) the computation and assembly of stiffness matrices corresponding to each layer and the underlying half-space of a multi-layered poroelastic half-space to establish eqn (76) for specified values of ξ and s corresponding to a given numerical Laplace inversion scheme; (2) the solution of eqn (76) to obtain the interlayer displacement and pore pressure vectors in the Laplace–Hankel transform space; (3) the evaluation of semi-infinite integrals with respect to ξ defined in eqn (9) by applying an adaptive version of an extended trapezoidal formula with a sampling interval of $\Delta \xi = 0.1$ and (4) the evaluation of the time-domain solutions by using eqn (77) or (79). It should be noted that the determinant of the global stiffness matrix is nonsingular along the integration axis of eqn (9) [i.e. real ξ axis for real values of s given by eqns (78) and (79)].

The numerical stability of the global stiffness matrix in eqn (76) for increasing values of ξ and s can be assessed by computing a condition number of the matrix (Cline *et al.*,

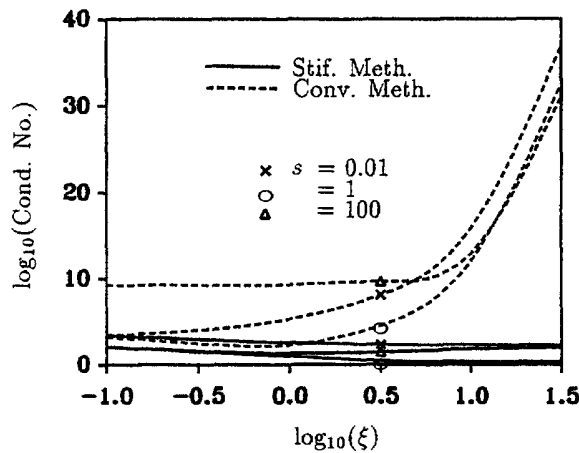


Fig. 2. Comparison of condition numbers corresponding to stiffness matrix and conventional method.

1979). Figure 2 presents L_1 -condition numbers (the multiplication of the first norm of a matrix and the first norm of its inverse) with respect to ξ for different values of s of the final equation systems corresponding to the present stiffness method [i.e. eqn (76)] and the conventional method based on the determination of layer arbitrary coefficients. The results shown in Fig. 2 correspond to a layered system consisting of a poroelastic layer of unit thickness ($v^{(1)} = 0.25, v_u^{(1)} = 0.35$ and $B^{(1)} = 0.8$) bonded to a poroelastic half-space ($v^{(1)} = 0.2, v_u^{(1)} = 0.3$ and $B^{(1)} = 0.6$). In addition, $\mu^{(1)}/\mu^{(2)} = 0.5$ and $\kappa^{(1)} = \kappa^{(2)}$. A coefficient matrix of a linear equation system with a small condition number is considered as a well-conditioned system whereas a large condition number indicates ill-conditioning. The numerical results in Fig. 2 show that the global stiffness matrix of the present scheme has a smaller condition number which either remains constant or decreases over a wider range of values of transform parameters, ξ and s . The condition number of the coefficient matrix corresponding to the conventional method is always higher than that of the global stiffness matrix of eqn (76) and becomes extremely large for increasing values of ξ due to the presence of mis-matching exponential terms in the coefficient matrix. The numerical stability of the present stiffness matrix approach is clearly demonstrated by the solutions shown in Fig. 2.

Table 1 presents a comparison of numerical solutions for vertical displacement and vertical stress at the point $(0, a)$ of a homogeneous poroelastic half-space ($v = 0.25, v_u = 0.35$ and $B = 0.8$) due to a uniform vertical patch load of radius “ a ” applied at a depth $z = a$ below the free surface. The half-space is considered to be consisting of 10 layers of equal thickness, $h/a = 0.2$, and an underlying half-space. Solutions obtained from the present

Table 1. Comparison of vertical displacement and vertical stress of a homogeneous poroelastic half-space ($v = 0.25, v_u = 0.35$ and $B = 0.8$) due to a uniform vertical patch load of radius “ a ” and uniform intensity f_0 acting at depth $z = a$

t^* (ct/a^2)	$2\mu u_z(0, a, t^*)/f_0 a$			$\sigma_{zz}(0, a^+, t^*)/f_0$		
	R & S† (1993)	Present study		R & S† (1993)	Present study	
		Stehfest	Schapery		Stehfest	Schapery
10^{-6}	0.9757	0.9757	0.9758	-0.7151	-0.7151	-0.7151
10^{-4}	0.9771	0.9771	0.9775	-0.7154	-0.7154	-0.7155
0.01	0.9891	0.9891	0.9910	-0.7181	-0.7181	-0.7179
0.1	1.0051	1.0051	1.0067	-0.7163	-0.7163	-0.7142
1.0	1.0271	1.0271	1.0291	-0.7059	-0.7059	-0.7068
10	1.0505	1.0505	1.0493	-0.7041	-0.7041	-0.7044
10^4	1.0635	1.0636	1.0635	-0.7040	-0.7040	-0.7040

† Rajapakse and Senjuntichai (1993).

stiffness method are compared with the numerical solutions given by Rajapakse and Senjuntichai (1993) to verify the numerical stability and the accuracy of the present technique. The solutions given by Rajapakse and Senjuntichai are obtained by numerically evaluating the explicit solutions for quasi-statics of a homogeneous poroelastic half-space and do not involve the application of the present matrix scheme. The two solutions are in excellent agreement. Table 2 presents a comparison of elastostatic solutions corresponding to a layer of unit thickness perfectly bonded to a half-space and subjected to uniform vertical pressure of unit total force applied over a circular area of unit radius at the top surface. Exact solutions (computed numerically) provided by Muki and Dong (1980) are used in the comparison with the final solutions ($t \rightarrow \infty$) from the present study. The general accuracy of the solutions obtained from the present stiffness matrix method are confirmed through these independent comparisons.

Numerical results for multi-layered poroelastic half-space

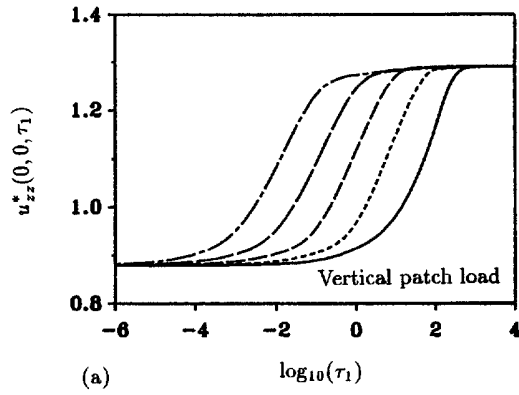
The quasi-static response of a multi-layered poroelastic half-space under a selected set of loadings is investigated in the numerical study. A layered system consisting of two poroelastic layers bonded to an underlying poroelastic half-space is considered in all numerical studies presented in this paper. The properties of the first layer are $B^{(1)} = 1.0$, $\nu^{(1)} = 0.25$ and $\nu_u^{(1)} = 0.5$; for the second layer, $B^{(2)} = 0.8$, $\nu^{(2)} = 0.25$ and $\nu_u^{(2)} = 0.35$ and for the underlying half-space, $B^{(3)} = 0.6$, $\nu^{(3)} = 0.2$ and $\nu_u^{(3)} = 0.3$. In addition, $\mu^{(2)}/\mu^{(1)} = 1$; $\mu^{(3)}/\mu^{(1)} = 2$ and applied loadings and fluid discharges are assumed to be uniformly distributed over a circular area of radius “ a ”.

Displacement histories due to surface loadings. Time histories of displacements at the origin ($r = 0, z = 0$) due to uniform patch loadings of intensity f_0 applied at the top surface are studied in this subsection. Problems of this nature are useful in the study of the consolidation settlement of surface foundations. In the parametric study, the total thickness of the two layers, $h_1 + h_2$, is equal to $2a$ and $\kappa^{(3)}/\kappa^{(2)} = 0.5$. A nondimensional time, $\tau_1 [= c^{(2)}t/a^2]$, in the range $10^{-6} \leq \tau_1 \leq 10^4$ is considered in the numerical study. Time histories of nondimensional vertical displacement, $u_{zz}^* [= 2\mu^{(1)}u_z/f_0a]$, at the origin due to a uniform vertical pressure are shown in Figs 3(a) and 3(c). Figures 3(b) and 3(d) present nondimensional horizontal displacement, $u_{xx}^* [= 2\mu^{(1)}u_x/f_0a]$, at the origin due to a uniform horizontal pressure applied at the top surface. Numerical results presented in Fig. 3 indicate that the general trend of the displacement histories are quite similar for both vertical and horizontal loadings. The influence of permeability on the response is considered in Figs 3(a) and 3(b) by setting $\kappa^{(1)}/\kappa^{(2)} = 0.001, 0.01, 0.1, 1.0$ and 10 with $h_1 = h_2 = a$. It can be seen from these two figures that the ratio $\kappa^{(1)}/\kappa^{(2)}$ has a significant influence on the consolidation process of a layered poroelastic half-space. As expected, the consolidation settlement is first noted in the case of $\kappa^{(1)}/\kappa^{(2)} = 10$ whereas, for $\kappa^{(1)}/\kappa^{(2)} = 0.001$, it is observed when $\tau_1 > 0.1$. The earliest final solution is reached for $\kappa^{(1)}/\kappa^{(2)} = 10$ and the latest for $\kappa^{(1)}/\kappa^{(2)} = 0.001$. This behaviour is due to the fact that the first layer is less permeable in the latter case. Comparison of displacement histories in Figs 3(a) and 3(b) indicates that the variation of the ratio $\kappa^{(1)}/\kappa^{(2)}$ essentially results in a shift of the response profile in the time scale. The numerical solutions in Figs 3(a) and 3(b) show identical initial and final

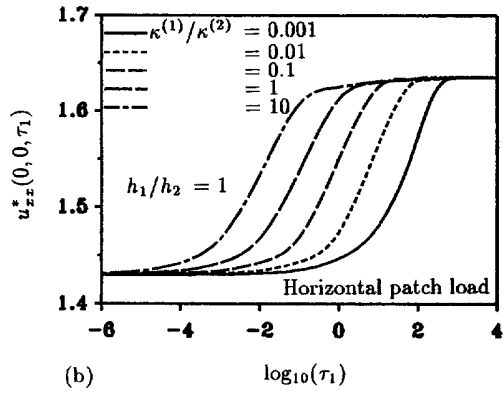
Table 2. Comparison of solutions for vertical displacement of a layered elastic half-space ($\mu^{(1)}/\mu^{(2)} = 10, \nu^{(1)} = \nu^{(2)} = 0.3$ and $h_1 = 1.0$) due to a uniform vertical patch load of intensity f_0 applied at the top surface

z	$2\mu u_z(0, z)$		r	$2\mu u_z(r, 0)$	
	M & D (1980)†	Present study		M & D (1980)†	Present study
0	0.1948	0.1948	0	0.1948	0.1948
1	0.1815	0.1813	1	0.1601	0.1600
2	0.1264	0.1262	2	0.1089	0.1088
6	0.0545	0.0542	5	0.0450	0.0448
11	0.0312	0.0308	10	0.0216	0.0215

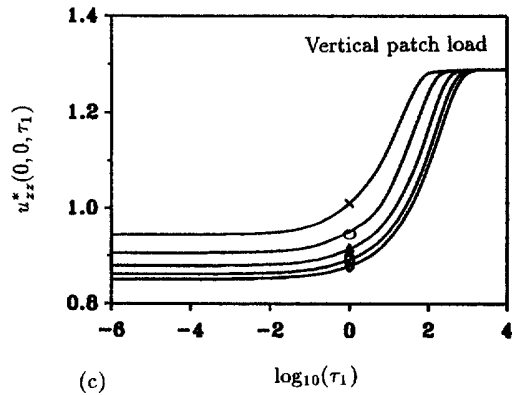
† Muki and Dong (1980).



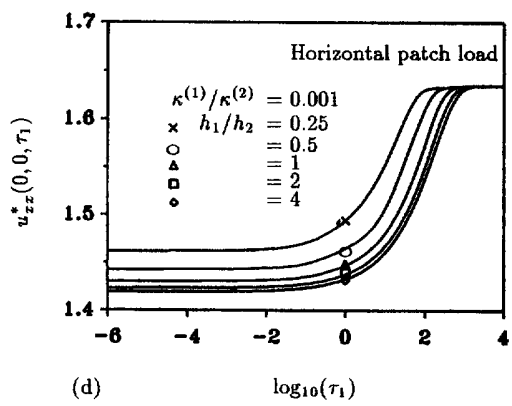
(a) $\log_{10}(\tau_1)$



(b) $\log_{10}(\tau_1)$



(c) $\log_{10}(\tau_1)$



(d) $\log_{10}(\tau_1)$

Fig. 3. Displacement histories due to surface loadings.

displacements since the material parameters, v , v_u and μ , and the thicknesses of the two layers are the same for all values of $\kappa^{(1)}/\kappa^{(2)}$.

The influence of layer thickness on the response is studied in Figs 3(c) and 3(d) for five different values of the ratio h_1/h_2 , i.e. $h_1/h_2 = 0.25, 0.5, 1, 2$ and 4 . Note that the total thickness of the two layers is $2a$ and $\kappa^{(1)}/\kappa^{(2)} = 0.001$. The initial displacements for different values of h_1/h_2 are different and their order of magnitude is identical to that of h_1/h_2 . This is a consequence of the fact that the undrained behaviour of poroelastic materials is mainly governed by the undrained Poisson's ratio, therefore a higher ratio of h_1/h_2 means a lesser undrained compressibility of the layered system since $v_u^{(1)} > v_u^{(2)}$. The consolidation settlements in all cases are initiated at almost identical time instants, i.e. after $\tau_1 > 0.1$, and the final settlement is first reached in the case where $h_1/h_2 = 0.25$ (i.e. $h_1/a = 0.4$ and $h_2/a = 1.6$) when $\tau_1 > 100$. It is also found that the time to reach the final solution increases with increasing values of h_1/h_2 . These features are consistent with the fact that since $\kappa^{(1)}/\kappa^{(2)} = 0.001$, the layered system becomes more impermeable for a higher ratio of h_1/h_2 . Final solutions are identical since elastic properties (drained) of the different layered systems are identical and the consolidation process in all cases is completed for $\tau_1 > 1000$.

Time histories of displacement and pore pressure due to fluid sink. The next set of solutions corresponds to problems involving fluid withdrawal from layered poroelastic media. Problems of this nature are useful in the study of settlement due to groundwater withdrawal, energy resource explorations, etc. A circular fluid sink of uniform intensity q_0 is located at the center of the second layer of the layer system defined previously. The sink is at a depth $z = 10a$ below the free surface. In the numerical study, the permeability of the first layer and the half-space is assumed to be equal, i.e. $\kappa^{(1)} = \kappa^{(3)}$, and the ratio $\kappa^{(2)}/\kappa^{(1)}$ is varied from 1 to 100. In addition, the thickness of the second layer is assumed to vary between a and $4a$. A nondimensional time, τ_2 where $\tau_2 = c^{(1)}t/a^2$, is used in the fluid sink problem. Time histories of nondimensional vertical displacement, $u_{zq}^* [= c^{(1)}u_z/q_0a^2]$, at the origin for different values of $\kappa^{(2)}/\kappa^{(1)}$ and h_2 are presented in Figs 4(a) and 4(b), respectively, for $10^{-2} \leq \tau_2 \leq 10^4$. It is found that the displacement at this point is higher than that at the point $(0, 10a)$ at all time instants. Similar behaviour was also observed in the numerical solutions reported by Rajapakse and Senjuntichai (1993) for the case of a buried patch fluid sink in a homogeneous poroelastic half-space. The solutions presented in Figs 4(a) and 4(b) indicate that the surface settlement in all cases is initially zero and increases rapidly with time during the period $1 < \tau_2 < 100$. Final solutions in all cases are reached when $\tau_2 > 1000$. Figures 4(c) and 4(d) show time histories of nondimensional pore pressure, $p_q^* [= c^{(1)}p/2\mu^{(1)}q_0a]$, at the center of the patch sink ($r = 0, z = 10a$) for different values of $\kappa^{(2)}/\kappa^{(1)}$ and h_2 , respectively, for $10^{-3} \leq \tau_2 \leq 10^3$. The initial pore pressure is zero and suction is subsequently developed at this point. Final values for suction are obtained after $\tau_2 > 100$. It is noted that less suction is developed due to a fluid sink in a more permeable layered system; i.e. for higher values of $\kappa^{(2)}/\kappa^{(1)}$ in Fig. 4(c) and for higher values of h_2 in Fig. 4(d). It can be argued that higher suction developed in a layered system results in higher stresses in the solid matrix (effective stresses) and consequently larger solid strains. Therefore, the solutions presented in Figs 4(a) and 4(b) indicate that the vertical displacement decreases with increasing values of $\kappa^{(2)}/\kappa^{(1)}$ and h_2 , respectively.

Pore pressure and fluid discharge profiles along the vertical axis. Nondimensional pore pressure, $p_z^* [= p/f_0]$, along the vertical axis due to a vertical patch load applied at the top surface are shown in Figs 5(a) and 5(b) for different values of $\kappa^{(1)}/\kappa^{(2)}$ and h_1/h_2 , respectively, for time instants $\tau_1 = 0.001$ and 1 . It is found that no suction is developed along the z -axis due to a vertical surface load and excess pore pressure becomes insignificant for $z > 4a$. The notable feature is that a discontinuity in the slope of the profiles is observed at the interfaces, i.e. at $z/a = 0.4$ for $h_1/h_2 = 0.25$, at $z/a = 1$ for $h_1/h_2 = 1$ and at $z/a = 1.6$ for $h_1/h_2 = 4$. This is due to the fact that since the permeability of the two layers are different a discontinuity exists in the slope of the pore pressure profiles at the interfaces. A small discontinuity also exists at the interface between the second layer and the half-space (i.e. at $z/a = 2.0$) since the permeability of the two media are not the same ($\kappa^{(3)}/\kappa^{(2)} = 0.5$). Initially

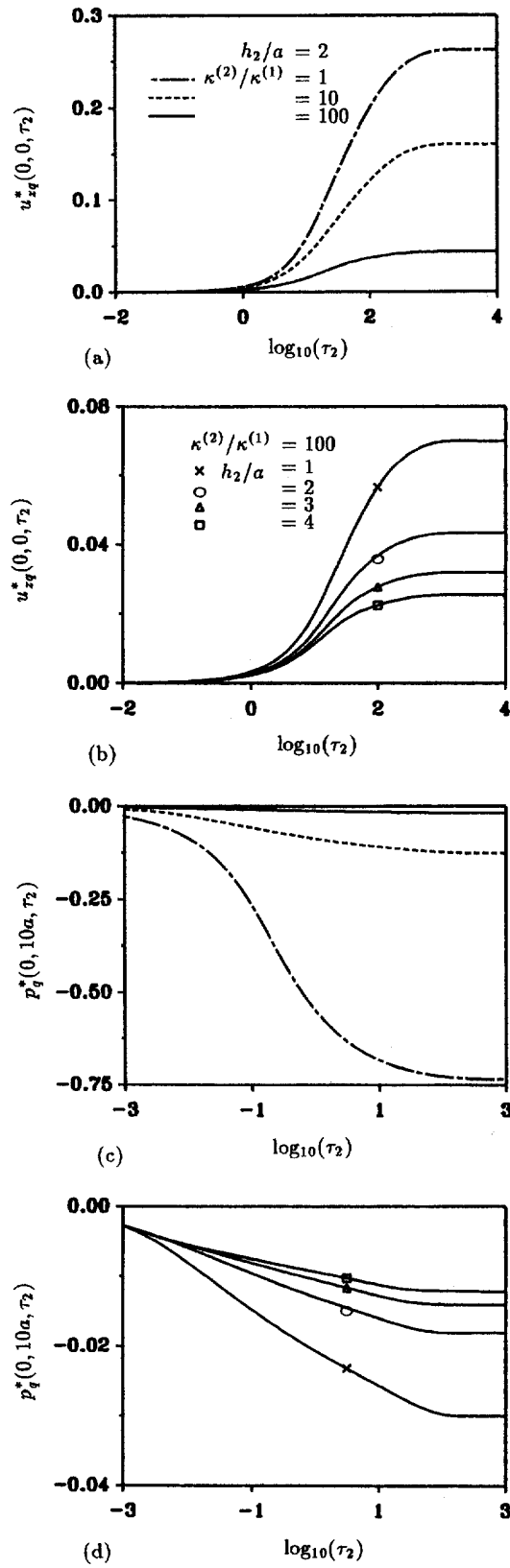


Fig. 4. Displacement and pore pressure histories due to a patch fluid sink.

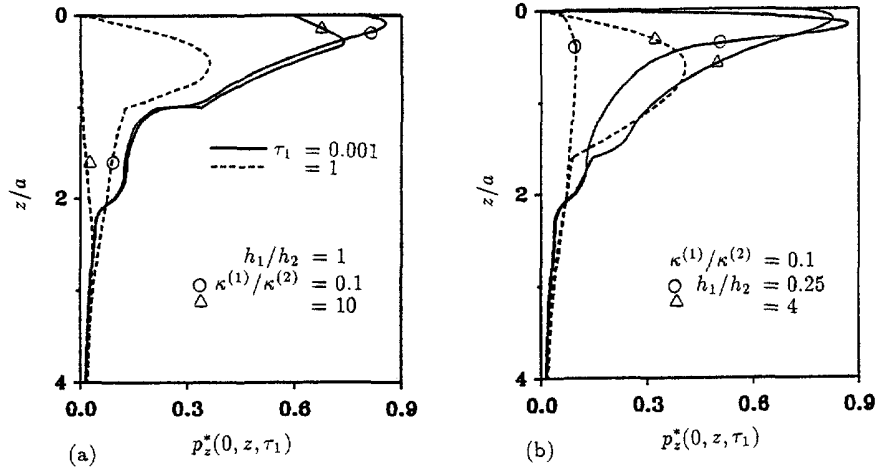


Fig. 5. Pore pressure along the z -axis due to a vertical patch load at the top surface.

($\tau_1 < 0.001$), a very large pore pressure is developed near the top surface resulting in a very high gradient of pressure in the region $0 < z/a < 1$. Pore pressure beneath the first layer decreases with depth in all cases and is nearly identical for $z/a > 2$. As expected, the rate of pore pressure dissipation increases with increasing values of permeability. For example, at $\tau_1 = 1$, excess pore pressure is nearly dissipated in the first layer for $\kappa^{(1)}/\kappa^{(2)} = 10$ whereas appreciable pore pressure is noted in the first layer if $\kappa^{(1)}/\kappa^{(2)} = 0.1$ for all values of h_1/h_2 . Excess pore pressure diminishes to negligible levels when $\tau_1 > 10$ and 100 for $\kappa^{(1)}/\kappa^{(2)} = 10$ and 0.1 , respectively.

Profiles of nondimensional pore pressure, p_q^* , and fluid discharge, $q_{zq}^* [= q_z/q_0]$, along the z -axis due to a patch fluid sink at a depth $z = 10a$ below the free surface are shown in Figs 6(a) and 6(b), respectively, for different time instants. Numerical solutions are presented for $8 \leq z/a \leq 12$ and for $\kappa^{(2)}/\kappa^{(1)} = 1$ and 10 when $h_2 = 2a$. Note that $\kappa^{(3)}$ is equal to $\kappa^{(1)}$ in this case. As expected, suction profiles shown in Fig. 6(a) indicate that the maximum value of suction is noted at the level of the sink (i.e. $z/a = 10$) for all values of τ_2 and the suction is higher for $\kappa^{(2)}/\kappa^{(1)} = 1$ when compared to $\kappa^{(2)}/\kappa^{(1)} = 10$. Naturally, the pore pressure profiles show a singularity (kink) at $z = 10a$ due to the fluid sink applied at this level. A discontinuity in the slope of the p_q^* profiles is observed at layer interfaces, i.e. at $z/a = 9$ and 11 for $\kappa^{(2)}/\kappa^{(1)} = 10$. Such a discontinuity does not exist for $\kappa^{(2)} = \kappa^{(1)}$. Final values for suction are attained when $\tau_2 > 1000$. Fluid discharge profiles shown in Fig. 6(b) for $\tau_2 = 0.1$ and 1000 indicate that a unit discontinuity exists at the level of applied patch fluid sink ($z = 10a$). A

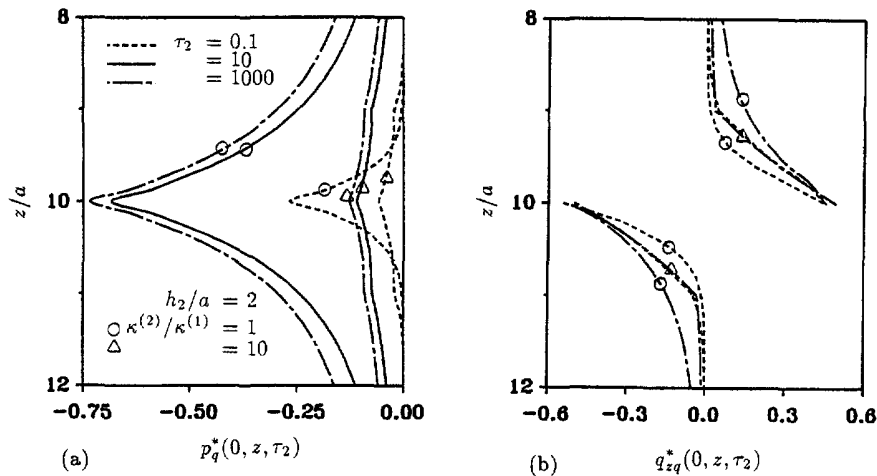


Fig. 6. Pore pressure and fluid discharge along the z -axis for a patch fluid sink.

discontinuity in the slope of the discharge profiles is also noted at $z/a = 9$ and 11 when $\kappa^{(2)}/\kappa^{(1)} = 10$ whereas, for $\kappa^{(2)} = \kappa^{(1)}$, discharge profiles are smooth along the z -axis. This behaviour is similar to that observed in Fig. 6(a). Initially ($\tau_2 < 0.1$), higher discharge is developed in the case where $\kappa^{(2)}/\kappa^{(1)} = 10$. As time increases, the discharge for $\kappa^{(2)} = \kappa^{(1)}$ increases and reaches a final state when $\tau_2 > 1000$. However, the discharge profile for $\kappa^{(2)}/\kappa^{(1)} = 10$ is nearly time-independent. The fluid discharge corresponding to both values of $\kappa^{(2)}/\kappa^{(1)}$ becomes negligible after $|z/a - 10| > 2$.

CONCLUSIONS

An exact stiffness matrix method based on three-dimensional analytical solutions of a homogeneous poroelastic medium is presented to study the quasi-static response of a multi-layered poroelastic half-space with compressible constituents. Displacements and pore pressure at layer interfaces in the Laplace–Hankel transform space are considered as the basic unknowns in the analysis. Explicit solutions for stiffness matrices of a layer with a finite thickness and a half-space are presented. These stiffness matrices need to be derived only once and can be applied to study the response of any horizontally layered poroelastic medium. The time domain solutions can be obtained by applying the numerical scheme proposed by Stehfest (1970) or Schapery (1962) for Laplace inversion and applying direct numerical quadrature to evaluate the Hankel transform inversion integrals. The present method has the advantage that the size of the final equation system is nearly one-half of that corresponding to the conventional matrix approach based on layer arbitrary coefficients. In addition, unlike the coefficient matrix of the conventional method, the global stiffness matrix of the present method is symmetric, numerically stable and well-conditioned for the large values of transform parameters and has a band width equal to eight. Selected numerical results presented in this study indicate that the response of a layered system is governed by many parameters (layer thickness, material parameters, etc.) and it is difficult to identify the influence of individual parameters separately on the response. The present method can be used to compute the kernel functions (Green's functions) required in the application of boundary integral equation methods for a multi-layered poroelastic half-space. It can also be used to verify the accuracy of approximate methods such as the finite element method and other numerical techniques that can be applied to study the consolidation problems involving layered poroelastic media.

Acknowledgements—The work presented in this paper was supported by the Natural Sciences and Engineering Research Council of Canada Grant A-6507.

REFERENCES

- Biot, M. A. (1941). General theory of three-dimensional consolidation. *J. Appl. Phys.* **12**, 155–164.
- Booker, J. R. and Small, J. C. (1987). A method of computing the consolidation behaviour of layered soils using direct numerical inversion of Laplace transforms. *Int. J. Numer. Anal. Meth. Geomech.* **11**, 363–380.
- Burmister, D. M. (1945). The general theory of stresses and displacements in layered soil systems. *J. Appl. Phys.* **16**, 89–94.
- Chan, K. S., Karasudhi, P. and Lee, S. L. (1974). Force at a point in the interior of a layered elastic half space. *Int. J. Solids Structures* **10**, 1179–1199.
- Choi, H. J. and Thangitham, S. (1991). Stress analysis of multilayered anisotropic elastic media. *J. Appl. Mech.* **58**, 382–387.
- Cline, A. K., Moler, C. B., Stewart, G. W. and Wilkinson, J. H. (1979). An estimate for the condition number of a matrix. *SIAM J. Numer. Anal.* **16**, 368–375.
- Detournay, E. and Cheng, A. H.-D. (1988). Poroelastic response of a borehole in a non-hydrostatic stress field. *Int. J. Rock Mech. Min. Sci. and Geomech. Abstr.* **25**, 171–182.
- Detournay, E., Cheng, A. H.-D., Roegiers, J.-C. and McLennan, J. D. (1989). Poroelastic consideration in *in situ* stress determination by hydraulic fracturing. *Int. J. Rock Mech. Min. Sci. and Geomech. Abstr.* **26**, 507–513.
- Haskell, N. A. (1953). The dispersion of surface waves on multilayered media. *Bull. Seism. Soc. Am.* **43**, 17–34.
- Kausel, E. and Peek, R. (1982). Dynamic loads in the interior of a layered stratum: an explicit solution. *Bull. Seism. Soc. Am.* **72**, 1459–1481.
- Kausel, E. and Seale, S. H. (1987). Static loads in layered halfspaces. *J. Appl. Mech.* **54**, 403–408.
- McNamee, J. and Gibson, R. E. (1960). Plane strain and axially symmetric problems of the consolidation of a semi-infinite clay stratum. *Q. J. Mech. App. Math.* **13**, 210–227.
- Muki, R. and Dong, S. B. (1980). Elastostatic far-field behavior in a layered half space under surface pressure. *J. Appl. Mech.* **47**, 504–512.

- Piessens, R. (1975). Bibliography on numerical inversion of the Laplace transform and applications. *J. Comp. Appl. Math.* **1**, 115–126.
- Rajapakse, R. K. N. D. (1993). Stress analysis of borehole in poroelastic medium. *J. Engng Mech.* **119**, 1205–1227.
- Rajapakse, R. K. N. D. and Karasudhi, P. (1985). Elastostatic infinite elements for layered half spaces. *J. Engng Mech.* **111**, 1144–1158.
- Rajapakse, R. K. N. D. and Senjuntichai, T. (1993). Fundamental solutions for a poroelastic half-space with compressible constituents. *J. Appl. Mech.* **60**, 844–856.
- Rajapakse, R. K. N. D. and Wang Y. (1992). Axisymmetric elastodynamic Green's functions of a layered transversely isotropic half space. *Proc. 14th Int. Conf. on Boundary Elements* **2**, 135–149.
- Rice, J. R. and Cleary, M. P. (1976). Some basic stress–diffusion solutions for fluid saturated elastic porous media with compressible constituents. *Rev. Geophys. Space Phys.* **14**, 227–241.
- Rudnicki, J. W. (1986). Slip on an impermeable fault in a fluid-saturated rock mass. In *Earthquake Source Mechanics* (Edited by J. Das, J. Boatwright and C. H. Scholz), Geophysical Monograph 37, pp. 81–89. American Geophysical Union.
- Rudnicki, J. W. (1987). Plane strain dislocations in linear elastic diffusive solids. *J. Appl. Mech.* **54**, 545–552.
- Schaperly, R. A. (1962). Approximate methods of transform inversion for viscoelastic stress analysis. *Proc. 4th U.S. Nat. Congress on Appl. Mech.* **2**, 1075–1085.
- Schiffman, R. L. and Fungaroli, A. A. (1965). Consolidation due to tangential loads. *Proc. 6th Int. Conf. Soil Mech. and Found. Engng* 188–192.
- Skempton, A. W. (1954). The pore pressure coefficients A and B. *Geotechnique* **4**, 143–147.
- Sneddon, I. N. (1951). *Fourier Transforms*. McGraw–Hill, New York.
- Stehfest, H. (1970). Numerical inversion of Laplace transforms. *Commun. Ass. Comput. Mach.* **13**, 47–49.
- Terzaghi, K. (1923). Die Berechnung der Durchlässigkeitziffer des Tones aus dem Verlauf der hydrodynamischen Spannungsercheinungen. *Sitzungsber. Akad. Wiss. Wien. Math.-Naturwiss. Kl., Abt. 2A* **132**, 105–124.
- Thomson, W. T. (1950). Transmission of elastic waves through a stratified solid medium. *J. Appl. Phys.* **21**, 89–93.
- Vardoulakis, I. and Harnpattanapanich, T. (1986). Numerical Laplace–Fourier transform inversion technique for layered-soil consolidation problems: I. Fundamental solutions and validation. *Int. J. Numer. Anal. Meth. Geomech.* **10**, 347–365.
- Waas, G. (1972). Linear two-dimensional analysis of soil dynamic problems in semi-infinite layered media. Ph.D. Thesis, University of California, Berkeley.
- Wang, Y. and Rajapakse, R. K. N. D. (1994). An exact stiffness method for elastodynamics of a layered orthotropic media. *J. Appl. Mech.*
- Wolfram, S. (1988). *Mathematica: A system for doing mathematics by computer*. Addison–Wesley Publishing Company, Inc.

APPENDIX

The matrices **R** and **S** in eqns (10) and (11), respectively, are given by

$$\mathbf{R} = [\mathbf{R}_1 ; \mathbf{R}_2] \quad (\text{A1})$$

$$\mathbf{S} = [\mathbf{S}_1 ; \mathbf{S}_2] \quad (\text{A2})$$

where

$$\mathbf{R}_1 = \begin{bmatrix} -2\mu a_3 \eta \delta_2 e^{\gamma z} & -2\mu a_3 \eta \delta_2 e^{-\gamma z} & a_1 z e^{\xi z} & -a_1 z e^{-\xi z} \\ 0 & 0 & 0 & 0 \\ 2\mu a_3 \eta \delta_1 e^{\gamma z} & -2\mu a_3 \eta \delta_1 e^{-\gamma z} & -(a_1 z - \frac{a_2}{\xi}) e^{\xi z} & -(a_1 z + \frac{a_2}{\xi}) e^{-\xi z} \\ 2\mu a_3 \eta e^{\gamma z} & 2\mu a_3 \eta e^{-\gamma z} & -2\mu a_4 \eta e^{\xi z} & -2\mu a_4 \eta e^{-\xi z} \end{bmatrix} \quad (\text{A3})$$

$$\mathbf{R}_2 = \frac{1}{2} \begin{bmatrix} e^{\xi z} & e^{-\xi z} & -e^{\xi z} & -e^{-\xi z} \\ e^{\xi z} & e^{-\xi z} & e^{\xi z} & e^{-\xi z} \\ -e^{\xi z} & e^{-\xi z} & e^{\xi z} & -e^{-\xi z} \\ 0 & 0 & 0 & 0 \end{bmatrix} \quad (\text{A4})$$

$$\mathbf{S}_1 = \mu \begin{bmatrix} -4\mu a_3 \xi \eta \delta_1 e^{\gamma z} & 4\mu a_3 \xi \eta \delta_1 e^{-\gamma z} & (2a_1 \xi z - 1) e^{\xi z} & (2a_1 \xi z + 1) e^{-\xi z} \\ 0 & 0 & 0 & 0 \\ 4\mu a_3 \xi \eta \delta_2 e^{\gamma z} & 4\mu a_3 \xi \eta \delta_2 e^{-\gamma z} & -2(a_1 \xi z - a_4) e^{\xi z} & 2(a_1 \xi z + a_4) e^{-\xi z} \\ -2a_3 \delta_1 e^{\gamma z} & 2a_3 \delta_1 e^{-\gamma z} & 2a_4 \delta_2 e^{\xi z} & -2a_4 \delta_2 e^{-\xi z} \end{bmatrix} \quad (\text{A5})$$

$$S_2 = \frac{\mu}{2} \begin{bmatrix} 2\xi e^{\xi z} & -2\xi e^{-\xi z} & -2\xi e^{\xi z} & 2\xi e^{-\xi z} \\ \xi e^{\xi z} & -\xi e^{-\xi z} & \xi e^{\xi z} & -\xi e^{-\xi z} \\ -2\xi e^{\xi z} & -2\xi e^{-\xi z} & 2\xi e^{\xi z} & 2\xi e^{-\xi z} \\ 0 & 0 & 0 & 0 \end{bmatrix} \quad (A6)$$

and

$$a_1 = \frac{1}{2(1-2\nu_u)}, \quad a_2 = \frac{(3-4\nu_u)}{2(1-2\nu_u)}, \quad a_3 = \frac{B(1+\nu_u)(1-\nu)}{3(\nu_u-\nu)}, \quad a_4 = \frac{(1-\nu_u)}{(1-2\nu_u)} \quad (A7)$$

$$c = 2\mu a_3 \kappa \eta, \quad \eta = \frac{B(1+\nu_u)}{3(1-\nu_u)}, \quad \delta_1 = \frac{\kappa \gamma \eta}{s}, \quad \delta_2 = \frac{\kappa \xi \eta}{s}. \quad (A8)$$